JAAS

Journal of Analytical Atomic Spectrometry

Accepted Manuscript

This article can be cited before page numbers have been issued, to do this please use: Z. Brubaker, S. Szakas, J. Hewitt, D. H. Moseley, D. T. Hoelzer and B. T. Manard, *J. Anal. At. Spectrom.*, 2026, DOI: 10.1039/D6JA00117C.

ROYAL SOCIETY OF CHEMISTRY

rsc.li/jaas

View Article Online
DOI: 10.1039/D6JA00117C

Microstructure-Dependent Particulate Populations in ODS Steels Revealed by Single-Particle ICP-TOF-MS

Z. E. Brubaker,* S. E. Szakas, J. Hewitt, D. H. Moseley, D. T. Hoelzer, and B. T. Manard
Oak Ridge National Laboratory, Oak Ridge, TN 37831

(Dated: May 27, 2026)

In this work, we evaluated the ability of single-particle inductively coupled plasma time-of-flight mass spectrometry (SP-ICP-TOF-MS) to characterize particulates generated from 300 series stainless steels and oxide dispersion–strengthened (ODS) steels. Particulates were produced using two different rotary tools (cutting disk and grinding bit) to assess the influence of particle generation on effluent particulates. Across all materials and preparation techniques, SP-ICP-TOF-MS detected a substantial population of particles containing the expected constituent elements, with average compositions closely matching the nominal alloy values. A secondary population of Y-bearing particles was evident in ODS steels; their formation is strongly favored in particulates generated using the grinding bit. Specifically, in PM2000, Y-bearing particles were predominantly colocated with Al, whereas in 14YWT, Y-bearing particles were less frequently Fe-free but showed stronger colocation with Ti. These trends are consistent with the known microstructural differences between Y–Al–O oxide particles in PM2000 and finer Y–Ti–O nanoclusters in 14YWT. Together, these results demonstrate that SP-ICP-TOF-MS can resolve distinct particulate populations in complex, multicomponent steels at the femtogram mass scale, enabling particle-resolved insight into microstructure-driven phase separation and preparation-dependent particle generation. [a]

INTRODUCTION

Single-particle inductively coupled plasma time-of-flight mass spectrometry (SP-ICP-TOF-MS) has emerged as a powerful tool for the elemental and isotopic characterization of submicron and nanoscale particulates [1–3]. In brief, particles are carefully introduced into the inductively coupled plasma (ICP) with the aim of ionizing single particles at a time. These ions are subsequently extracted into the time-of-flight (TOF) mass spectrometry (MS) instrument, which collects a full mass spectrum for each transient ion cloud. Therefore, SP-ICP-TOF-MS enables quasi-simultaneous, multielement detection at the single-particle level with high throughput. Owing to its relatively modest per-sample cost, minimal sample preparation requirements, and high analytical value, SP-ICP-TOF-MS has been increasingly applied to environmental, biological, and nuclear forensics samples [3–12].

Much of the literature has focused on compositionally simple nanoparticles such as Au, Ag, CeO_2, and TiO_2, for which signal interpretation and detection limits are well established [1, 4, 13–18]. In parallel, an increasing number of studies have applied SP-ICP-TOF-MS to chemically complex particulates containing multiple elements, including multimetal and composite systems [5, 6, 8, 9, 19–26]. These studies have demonstrated the capability of SP-ICP-TOF-MS to resolve multielement nanoparticles and heterogeneous particulate populations; at the same time, they have also underscored the importance of careful interpretation of detection limits, elemental colocation, and particle classification in complex matrices.

For steels or steel-related particulates, relatively few studies have been reported [20–24]. These studies have demonstrated that particulates consistent with steel compositions can be detected in environmental settings, with measured elemental ratios generally in good agreement with expected source terms. To date, however, studies have focused primarily on compositionally homogeneous steels, and the influence of particle-generation mechanisms has not been systematically examined. Particles generated during cutting, grinding, and other mechanical processing operations are ubiquitous in manufacturing environments, span the submicron to nanoscale size range, and may exhibit substantial chemical heterogeneity [27]. Particle-resolved compositional analysis is therefore important for exposure assessment and process monitoring.

Whereas 300 series stainless steels are primarily Fe–Cr–Ni alloys, oxide dispersion–strengthened (ODS) steels are nominally Ni-free, but also contain additional alloying elements that complicate particulate composition and microstructural homogeneity. ODS steels, which have been developed for fission and fusion environments, contain a high number density of nanoscale Y-bearing oxide precipitates embedded within the Fe-rich matrix [28–32]. These oxide precipitates are critical to creep strength and radiation tolerance but constitute minor phases (< 1 wt.%) compared to the metallic matrix. Although electron microscopy–based techniques are well suited for resolving nanoscale heterogeneity and phase identity, they are typically applied to relatively small particle populations. As a result, complementary high-throughput approaches are valuable for establishing statistically representative particle distributions.

In this work, we developed and demonstrated an SP-ICP-TOF-MS workflow for the analysis of complex, composite

[a] Notice: This manuscript has been authored by UT-Battelle, LLC, under contract DE-AC05-00OR22725 with the US Department of Energy (DOE). The US government retains and the publisher, by accepting the article for publication, acknowledges that the US government retains a nonexclusive, paid-up, irrevocable, worldwide license to publish or reproduce the published form of this manuscript, or allow others to do so, for US government purposes. DOE will provide public access to these results of federally sponsored research in accordance with the DOE Public Access Plan (http://energy.gov/downloads/doe-public-access-plan).

View Article Online
DOI: 10.1039/D6JA00117C

metal particulates. We used two complementary material classes: (i) particulates generated from 300 series stainless steels (304L and 316L) as a benchmark system for routine multielement particles, and (ii) particulates generated from ODS steels as a demanding test case for minor element detection and to assess whether the distinct Y-bearing phases separate from the underlying Fe-based matrix. By applying particle-resolved detection limits and colocation analysis, we evaluated the extent to which SP-ICP-TOF-MS can distinguish matrix- and oxide-derived particulates and resolve preferential elemental associations in chemically heterogeneous steel systems.

EXPERIMENTAL METHODS

Materials

The investigated materials were 304L, 316L, 14YWT, and PM2000 steels. The nominal compositions are shown in Table I. The 304L and 316L steels were obtained from McMaster-Carr, the 14YWT steel was obtained internally at Oak Ridge National Laboratory, and the PM2000 steel was obtained from Plansee GmbH, Austria.

Both 14YWT and PM2000 steels exhibit distinct microstructures that directly influence the distribution of minor alloying elements [28–30]. Both materials contain a high number density of nanoscale oxide features formed during mechanical alloying and subsequent consolidation; however, the composition, size, and spatial distribution of these features differ substantially between the two alloys.

PM2000 is a ferritic Fe–Cr–Al ODS steel produced by Plansee for use in heat exchangers in the fossil energy industry because of its high-temperature oxidation resistance and creep performance. [35]. In PM2000, Y is predominantly incorporated into Y–Al–O oxide particles; $YAlO_3$ is the primary particulate phase [28, 30]. Previous electron microscopy and atom probe tomography studies have shown that these oxide particles are relatively coarse and typically have diameters of about 10–25 nm, although some studies have reported particle sizes exceeding 50 nm [28–30, 36]. Titanium is present at low concentrations, but the presence of Al prevents the formation of Y–Ti–O phases and results in Ti being distributed throughout the matrix. However, some studies have found a Ti shell around Y–Al–O clusters [28, 30]. As a result, Y–Al–O particles in PM2000 represent a chemically distinct secondary phase embedded within an Fe-rich metallic matrix.

In contrast, 14YWT is a ferritic–martensitic ODS steel developed at Oak Ridge National Laboratory for use in advanced nuclear energy reactor fuel cladding and core internals that require high-temperature strength and creep properties that resist degradation in extreme neutron irradiation environments at high temperatures and high neutron doses [33, 34]. The 14YWT alloy was specifically engineered to promote the formation of fine Y–Ti–O nanoclusters [31, 32]. In this alloy, both Y and Ti are strongly associated with oxide precipitates that are significantly smaller than those in PM2000, typically ranging from approximately 1 to 5 nm in diameter [29, 31]. Although the highest number density is evident for this size range, note that a smaller number of 5–20 nm Y–Ti–O clusters have also been reported [33, 37].

Sample Preparation

Because the characteristics of generated particulates depend on the preparation method, two complementary techniques—cutting and grinding—were employed [27].

Particles were generated using a rotary tool, 60 mL Savillex jars, and 3D printed, custom-designed jar tops to hold the alloys and seal the opening. An alloy piece was fixed to a jar top and then placed over the opening of a Savillex jar containing 10 mL of 18 MΩ·cm water. The rotary tool was then used to abrasively cut or grind the surface of the alloy for 60 s. For each sampling jar, the rotary tool was fitted with a ceramic cutoff wheel (McMaster-Carr 1257A15 rotary tool cutoff wheel, 7/8 in. diameter, 0.009 in. thick) for cutting and an aluminum oxide grinding bit (McMaster-Carr 4393A98 grinding bit for metals, 1/8 in. shank diameter, shape no. B42, 46 grit) for grinding. After sample generation, the lids were rinsed with 18 MΩ·cm water to extract any residual particles still on the lid. The resultant samples were diluted an additional 40x for SP-ICP-TOF-MS measurements.

To minimize aggregation during sample preparation, samples were briefly sonicated for 10 s, allowed to settle for 10 min, and subsequently pipetted from the top of the sample jar to avoid visible debris and larger particulates that had settled to the bottom.

SP-ICP-TOF-MS

An ICP-TOF-MS instrument (icpTOF R, TOFWERK AG, Switzerland) was employed for detecting single alloy particles. Particle mass was determined via external calibration-based quantification using multielement standards (High Purity Standards, Charleston, SC, USA) and monodisperse spherical Au nanospheres (100 nm, nanoComposix, Fortis Life Sciences, San Diego, CA, USA). Samples were diluted in ASTM type I water (18.3 MΩ·cm) generated with a Thermo Scientific Barnstead GenPure xCAD Plus ultrapure water purification system (Waltham, MA, USA). For high-efficiency particle introduction, samples and standards were introduced into the ICP-TOF-MS instrument using a microFAST SingleCell sample introduction system (Elemental Scientific Inc. [ESI], Omaha, NE, USA) with a CytoNeb200 nebulizer (ESI) housed within a CytoSpray chamber (ESI, SC-CytoC-73) [38].

All data were processed using TOF-SPI (TOF single particle investigator), an open-source batch analysis program written in LabVIEW (LabVIEW 2018, National Instruments, TX,

View Article Online
DOI: 10.1039/D6JA00117C

	Composition (wt.%)									Particle count	
Material	Fe	Cr	Ni	Mn	Mo	Al	Ti	Y	W	Disk	Grind
304L	69.6 ± 4.9	18.75 ± 1.25	10 ± 2	1 ± 1	—	—	—	—	—	4,251	7,863
316L	69.5 ± 2.5	17 ± 1	11 ± 1	1 ± 1	2.5 ± 0.5	—	—	—	—	1,149	18,406
14YWT	82.4	14	—	—	—	—	0.4	0.2	3	23,634	6,626
PM2000	74	19.5	—	—	—	5.5	0.5	0.4	—	927	5,141

TABLE I. Manufacturer-provided (304L and 316L) or reported (14YWT [33, 34] and PM2000 [35]) nominal alloy compositions and total particle counts detected by SP-ICP-TOF-MS for each preparation method, summing both runs. The composition ranges for 304L and 316L are based on vendor specifications.

USA). TOF-SPI enables calculation of element-specific critical values (L_C), which are defined as the minimum signal that can be distinguished from background (i.e., baseline signal) and attributed to a particle-derived event[39]. For each analytical run, L_C was calculated independently. The resulting L_C ranges are provided in Table II.

Using the measured dissolved background and the calculated L_C values, data were background-subtracted and corrected for split events. Calibration was performed using a particle standard and the appropriate calibration curve to determine absolute elemental sensitivities [40, 41]. From these sensitivities, the mass of each monitored element and isotope within the individual particle events was calculated. Although the TOF analyzer records all mass channels simultaneously, we used only the isotopes listed in Table II in this analysis. Minor isotopes of Fe and Cr (i.e., ^{57}Fe and ^{53}Cr instead of ^{56}Fe and ^{52}Cr) were selected to minimize common polyatomic interferences in ICP-MS analysis.

All samples were analyzed in duplicate with 300 s acquisition times. Transport efficiency was approximately 50%. We note that the transport efficiency is likely somewhat size dependent, with smaller particulates having higher transport efficiencies. Therefore, some of the data may be slightly biased towards smaller particulates. That said, as will be discussed later, analysis involving elemental ratios was thresholded, which helps eliminate bias in the ratio due to size. Table I lists the total number of detected particles for each material and preparation method.

In both ODS steels, the majority of Y-bearing nanoclusters were expected to fall below the detection limit of SP-ICP-TOF-MS(Table II). Even under the assumption that the oxide inclusions consist solely of Y_2O_3 with a density of 5.01 g·cm^{-3}, a spherical nanocluster with a diameter of 5 nm (representative of 14YWT) would contain at most about 0.26 ag of Y, and a 25 nm inclusion (representative of PM2000) would contain approximately 32 ag of Y. Both values are significantly less than the single-particle detection threshold. A 37 nm Y_2O_3 nanocluster would be required to exceed the largest L_C measured in this work (104 ag). Consequently, direct detection by SP-ICP-TOF-MS likely reflects the aggregation of multiple nanoclusters or the detection of larger oxide inclusions.

Isotope	L_C range (fg)
^{27}Al	1.80–4.76
^{48}Ti	0.386–0.742
^{53}Cr	2.66–3.31
^{55}Mn	0.225–0.584
^{57}Fe	18.4–24.4
^{60}Ni	1.28–2.32
^{89}Y	0.063–0.104
^{95}Mo	0.463–0.577
^{182}W	0.070–0.140

TABLE II. Range of isotope-specific critical values (L_c)

RESULTS AND DISCUSSION

Figure 1 shows the relative detection frequency of elements expected in the investigated steels for both particle preparation techniques. For the austenitic 300 series stainless steels, Fe, Cr, Ni, and Mn were detected consistently. Molybdenum was frequently detected in 316L, in agreement with the alloy's nominal composition. Molybdenum was less frequently detected in 304L (although it was detected more often than it was in ODS steels); this result suggests that the investigated 304L steel may have contained a small amount of Mo. Other elements not nominally contained in these steels, including Y, were detected with varying frequencies.

In the ODS steels, Fe, Cr, and W (14YWT only) were regularly detected. Yttrium was regularly detected in PM2000 but was less common in 14YWT. For 14YWT particles prepared with the cutting disk, Y detection was comparable to Y detection in 316L; in contrast, Y was detected more frequently in 14YWT particles generated using the grinding bit.

Aluminum and Ti also exhibited different behavior depending on the preparation technique. When particles were generated using the grinding bit, Al and Ti were detected at relatively constant frequencies across all materials, suggesting that a significant fraction of these particulates originated from the grinding media. In contrast, particles generated using the cutting disk exhibited highly variable Al and Ti detection frequencies: 304L and 316L had substantial Al- and Ti-bearing particulate populations that were inconsistent with

View Article Online
DOI: 10.1039/D6JA00117C

their nominal compositions; PM2000 had an elevated Al detection frequency consistent with its composition but complicated by contributions from particle preparation; and 14YWT exhibited comparatively low Al and Ti detection frequencies. The 14YWT samples also had a higher Fe-bearing particulate fraction when prepared with the cutting disk, coincident with a reduction in Al-bearing particles. Therefore, disentangling source material from preparation-induced background and evaluating particulate compositions requires a nuanced approach.

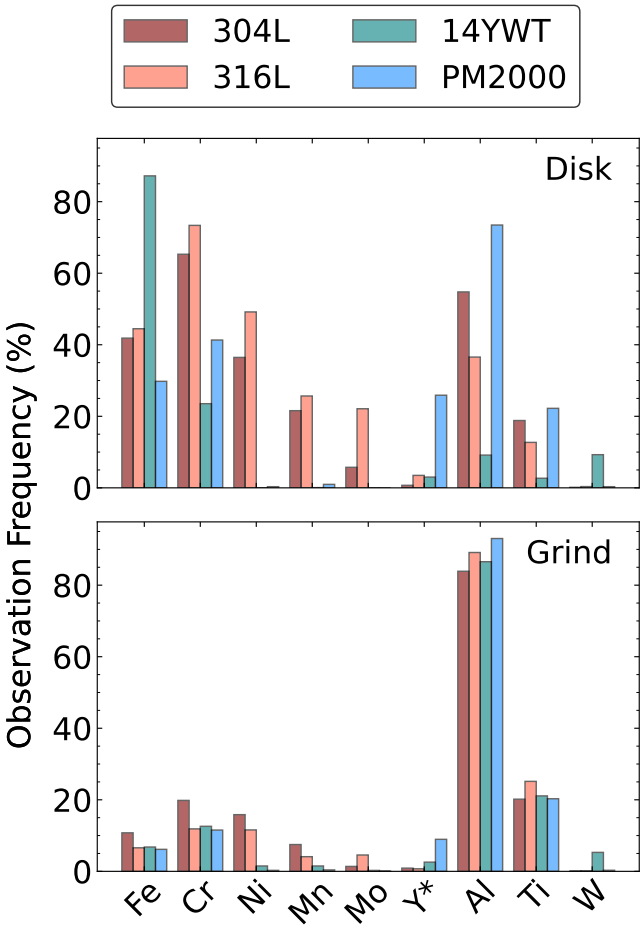

FIG. 1. Relative detection frequencies of select elements for all steels and both preparation techniques. The Y detection frequency (marked Y*) is multiplied by 10 for visual clarity. All expected elements were detected. Aluminum and Ti were detected at elevated frequencies in samples prepared using the grinding bit, indicating substantial contributions from the preparation method.

To this end, we first examine the Fe–Cr content, which represent the major elements in each steel. Figure 2 shows the Fe:Cr ratio as a function of Fe counts for particles generated using the grinding bit and cutting disk. For particles generated using the grinding bit, the majority of detections fall within the confidence intervals (dashed orange/green lines) predicted by counting (Poisson) statistics. At the lowest Fe counts, an increased number of outliers are evident, consistent with additional sources of uncertainty becoming more influential at low signal levels.

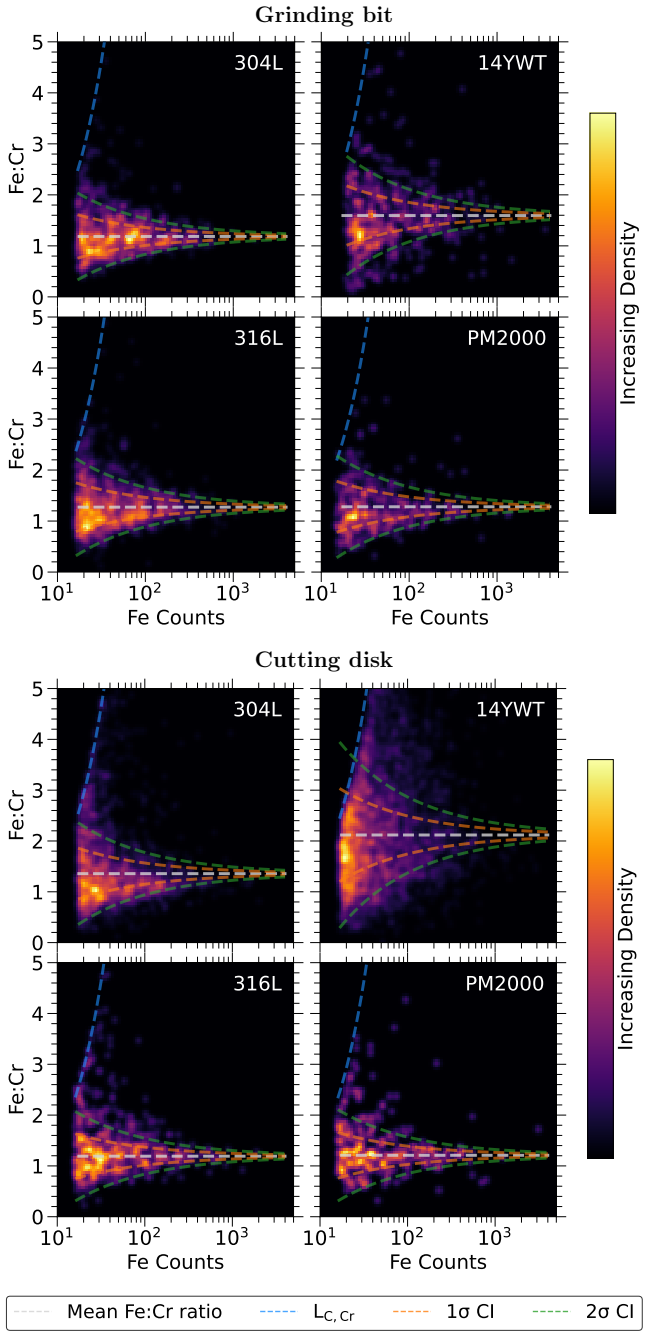

FIG. 2. The Fe:Cr ratio plotted against Fe counts for all particulates generated using the grinding bit (top) and cutting disk (bottom). To reduce the effect of the Fe-rich particulates evident at low Fe counts and to assess whether the observed distribution was consistent with counting statistics, the mean was calculated only from particles containing more than 10% of the maximum number of Fe counts. The 1σ and 2σ confidence intervals derived from counting statistics are indicated by the dashed orange and green lines, respectively.

Particulates generated from the cutting disk show different behavior. Although many particles remain consistent with

View Article Online
DOI: 10.1039/D6JA00117C

counting statistics, a larger population of Fe-rich outliers is evident. This effect is most pronounced for 14YWT and, to a lesser extent, 304L. The spread is largest at low Fe counts and broadly follows the Cr detection boundary (dashed blue lines), indicating that detection limitations contribute to but may not fully explain the distribution. To assess whether this scatter (or heterogeneity) arose from an external particle source associated with the cutting disk, we separated particles based on the presence of Y in 14YWT (see the supplementary information). Even under this constraint, the excess data spread beyond counting statistics persisted, indicating that the effect could not be attributed solely to contamination from the preparation method.

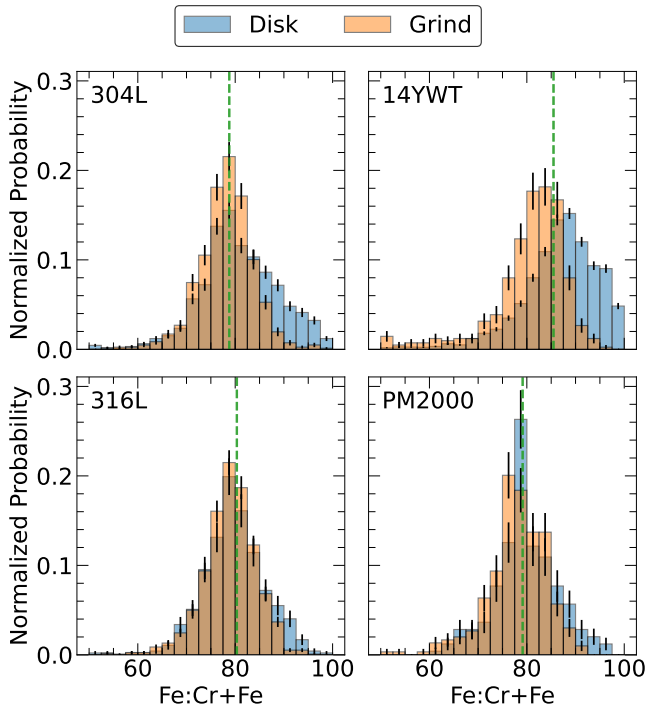

FIG. 3. The Fe:Cr+Fe ratio distributions for each material and preparation technique. Most distributions exhibit a single, sharp peak. The 304L and 14YWT particles generated using the cutting disk show pronounced asymmetry toward Fe-rich compositions.

Figure 3 shows the Fe:Cr+Fe distributions for each material and preparation technique. All materials exhibit peak probability densities near the expected values based on their nominal compositions. However, 304L and 14YWT particles prepared using the cutting disk show asymmetric distributions with extended intensity toward Fe-rich compositions, consistent with the presence of the Fe-rich outliers evident in Fig. 2.

Whether less abundant elements are detected consistently and near the expected composition requires careful particle-resolved analysis. The heterogeneous microstructure of the ODS steels may facilitate partial separation of oxide phases from the metallic matrix, potentially giving rise to distinct particle populations, independent of sample preparation method; in contrast, no such behavior is expected for the compositionally homogeneous 300 series stainless steels.

To evaluate this possibility, we must determine the minimum particle mass required to detect all constituent elements with a specified confidence. Thus, we use L_C values to calculate the minimum signal that results in reliable element detection;

$$L_{D,sp,M} = \left(\frac{z_{1-\beta} + \sqrt{(z_{1-\beta})^2 + 4L_{C,sp,M}}}{2} \right)^2, \qquad (1)$$

where $L_{C,sp,M}$ is the detection limit of element or isotope M, and $z_{1-\beta}$ is the z-score for a normal distribution [42, 43]. Here, we use a 95% confidence level, $z_{0.95} = 1.64$. The L_C value is dictated by the false positive rate, whereas the L_D value is dictated by the false negative rate.

Because Fe is the dominant element in all four materials, we convert $L_{D,sp,M}$ to the Fe counts necessary to detect element M, $L_{D,sp,Fe,Fe-M}$, using the nominal count ratio $R_{Fe:M}$:

$$L_{D,sp,Fe,Fe-M} = L_{D,sp,M} R_{Fe:M} \qquad (2)$$

where $R_{Fe:M}$ is calculated from the compositions shown in Table I by converting these values to counts. The $L_{D,sp,Fe,Fe-M}$ value is calculated for each constituent element of a given steel, and the maximum value defines the minimum Fe counts required to detect all constituent elements with 95% confidence. These counts are subsequently converted to a minimum detectable Fe mass.

Table III summarizes the resulting detection thresholds and detection efficiencies for selected element combinations. The L_C value was determined independently for each experimental run, and each sample/preparation was run in duplicate. Note that the L_D values reported in Table III represent the average value for both runs, but individual L_D values were used in assessing the confidence level.

In the 300 series stainless steels, particulates generated using the grinding bit had detection efficiencies near the expected 95% confidence level for all constituent elements. In contrast, particulates produced using the cutting disk had substantially lower detection efficiencies, a result that may be connected to the increased abundance of Fe-rich particulates discussed previously. As expected, detection efficiency for Fe–Cr, specifically, was high for both preparation methods, although it was still suppressed for cutting disk–generated particulates.

For ODS steels, the overall detection efficiency was less than 30% for both preparation techniques. Nevertheless, detection efficiency for Fe–Cr was high for particulates generated using the grinding bit (>95%), although some suppression was evident for disk-prepared samples. With the exception of cutting disk–generated 14YWT particles, which had the highest relative detection frequency of Fe-rich particulates (Fig. 2), the most frequently missed element was Y.

View Article Online
DOI: 10.1039/D6JA00117C

Material	Method	M	$L_{D,sp,Fe,Fe-M}$ (fg)	N_{Fe}	% All	% Fe–Cr	% All\Y	% All\Ti
304L	Disk	Mn	48.5	842	73.2	88.9	—	—
	Grind	Mn	45.3	493	95.8	97.5	—	—
316L	Disk	Mn	56.2	212	69.8	92.5	—	—
	Grind	Mn	55.6	512	89.6	97.0	—	—
14YWT	Disk	Ti	246.0	698	18.4	70.2	22.0	30.1
	Grind	Ti	161.8	96	26.0	99.0	60.4	28.1
PM2000	Disk	Ti	154.2	50	30.0	85.7	56.0	32.0
	Grind	Ti	114.3	64	20.3	97.8	61.0	23.4

TABLE III. Combined detection statistics for particle compositions. Detection limits (L_D) are reported as the average of the two runs for each experiment; N_{Fe} is the number of particles above L_D; % All and % Fe–Cr are the fractions of particles above L_D containing all constituent steel elements or Fe and Cr, respectively; and %All\Y and %All\Ti are the fractions of particles above L_D that contain all constituent elements except for Y or Ti, respectively.

Although this result was partially influenced by the elevated preparation-induced background associated with Ti and Al, it nonetheless suggests that Y is less abundant in Fe-based particulates than would be expected based on the nominal composition. We speculate that this apparent separation arises from the heterogeneous microstructure of ODS steels. Because Y is preferentially incorporated into oxide-based nanoclusters, it would be unsurprising if some of these clusters separate from the Fe matrix during particle preparation.

To investigate this possibility, we evaluated Y-bearing particulates that did *not* contain Fe, using this population as a metric to bound Y separation from the broader matrix (Table IV). We also included 304L and 316L, which do not nominally contain Y, to bound the effect and chemistry of impurity Y-bearing particulates.

In PM2000, the majority of Y-bearing particulates were detected in the absence of Fe; 87% of Y-bearing particles generated using the grinding bit lacked Fe. In 14YWT, nearly half of all Y-bearing particulates generated using the grinding bit lacked Fe. For both materials, the use of the cutting disk increased the apparent colocation of Y and Fe.

In PM2000, Y was most frequently found in association with Al and much less frequently with Ti. Because Al represents the most significant preparation-induced background in these measurements, we also assessed the probability of Y–Al colocation in 304L, 316L, and 14YWT by applying the same Y:Al ratio used for PM2000 in Eq. 2 as a control. Even under this assumption, Y–Al associations in PM2000 far exceeded those in the other materials, indicating that Y–Al coupling is intrinsic to PM2000 rather than being an artifact of preparation-induced background contributions.

However, Y–Ti associations are less clear. Colocation of Y–Ti was frequent in 304L and 316L, which nominally contain neither element, indicating that this pairing may arise from polyatomic interferences or preparation-induced background contributions. Therefore, the colocation of Y and Ti in 14YWT is more difficult to interpret.

Nevertheless, the aggregate trends were consistent with established differences in the oxide nanocluster populations of the two ODS steels [28–32]. In PM2000, oxide nanoclusters are known to be primarily composed of Y–Al–O; Ti largely remains in solid solution within the ferritic matrix or contributes only secondarily to oxide chemistry. These nanoclusters are relatively large, with characteristic diameters of 15–25 nm or larger, and they may separate from the surrounding metallic matrix during mechanical material removal. Although the detection limit of SP-ICP-TOF-MS exceeds the mass of a single nanocluster, occasional detection of colocated or larger aggregates is plausible and consistent with elevated Y–Al detection frequency.

By contrast, 14YWT contains finer, more uniformly dispersed oxide populations that incorporate both Y and Ti [29–31, 33]. The dominant Y-bearing nanoclusters in 14YWT are only a few nanometers in diameter and are closely embedded within the ferritic matrix. The relatively frequent colocation of Y with Fe in 14YWT is potentially a direct consequence of the detection limits of SP-ICP-TOF-MS–only particulates containing a large number of Y nanoclusters are detectable, but these particulates necessarily also contain Fe. However, the frequent detection of Fe without Y may arise from a lower overall Y-content in Fe-bearing particulates compared to the nominal composition.

Under this framework, the Y-bearing particulates detected without Fe may represent less common events, such as the liberation of larger or aggregated Y–Ti–O clusters. Features such as $Y_2Ti_2O_7$ with reported diameters of 19.8 $\pm$ 7.6 nm [33] fall within a size regime in which separation and detection of larger aggregates become plausible. However, interpretation of Y–Ti associations remains complicated by the frequent Y–Ti pairing detected in the 300 series stainless steels, indicating that some fraction of these associations may arise from polyatomic interferences or preparation-induced background effects. Nonetheless, the higher abundance of Y-bearing particles in 14YWT, together with its distinct Y–Fe and Y–Al association trends relative to the 300 series stainless steels, supports the conclusion that a meaningful portion of detected

View Article Online
DOI: 10.1039/D6JA00117C

Material	Method	Y–Fe			Y–Al\Fe			Y–Ti\Fe		
		L_D (fg)	N_Y	%Y\Fe	L_D (fg)	N_Y	% Y–Al\Fe	L_D (fg)	N_Y	% Y–Ti\Fe
304L	Disk	0.08	32	87.5	0.39	11	45.4	0.52	9	100
	Grind	0.08	65	86.2	0.26	21	38.1	0.42	15	93.3
316L	Disk	0.07	15	87.7	0.41	5	40.0	0.54	4	100
	Grind	0.07	143	97.2	0.30	49	63.3	0.40	38	94.7
14YWT	Disk	0.08	1639	21.7	0.44	45	8.9	0.60	37	84.1
	Grind	0.08	242	48.8	0.21	48	49.7	0.39	24	91.7
PM2000	Disk	0.16	224	63.8	0.37	41	85.6	0.83	14	28.6
	Grind	0.15	694	87.0	0.20	433	92.7	0.62	85	30.7

TABLE IV. Combined Y–*M* association statistics. The $L_{D,sp,Y,Y-M}$ value was calculated for M = Fe, Al, and Ti; N_Y denotes the number of Y-bearing particles above the associated L_D; %Y\Fe is the percentage of Y-bearing particulates above L_D that do not contain Fe; % Y–Al\Fe and %Y–Ti\Fe are the percentages of Y-bearing particulates above the associated L_D that contain Al or Ti, respectively, and do not contain Fe. Reported L_D values are the mean of the two runs. Although 14YWT does not contain Al, the Y:Al ratio used to calculate L_D for PM2000 was applied as a control to assess preparation-induced background contributions. Similarly, the L_D values for the 300 series stainless steels were calculated using the same ratios that were used for 14YWT.

Y–Ti events reflect intrinsic oxide features rather than purely background-driven coincidences.

The particulate generation mechanism further influences the detected populations. For both ODS steels, particulates generated using the cutting disk were considerably more likely to be colocated with Fe than particulates generated using the grinding bit. Therefore, layer-by-layer removal using the grinding bit seems to favor removal of nanoclusters from the matrix, whereas the cutting disk is less likely to liberate these nanoclusters.

Finally, we evaluated the average composition of particulates that contain all elements for a given steel above $L_{D,sp,Fe,Fe-M}$ (Fig. 4). In the 300 series stainless steels, all elements were quantified within the expected range of the nominal composition and within the uncertainties obtained from SP-ICP-TOF-MS. In 14YWT, the W content was slightly underestimated for materials prepared using the cutting disk, and significant variation is evident in the Ti content, likely because of the significant Ti background, potentially arising from particle preparation or polyatomic interferences. In PM2000, large standard deviations resulting from the significant preparation-induced background are evident for Al and Ti, and Ti may be subject to polyatomic interferences. Yttrium tends to be underestimated, consistent with the hypothesis that some nanoclusters separate from the metallic matrix during particle generation. If we do not restrict the particles to contain Fe above $L_{D,sp,Fe,Fe-M}$, then the composition and spread extracted for Ti and Al differ substantially from their nominal compositions. Overall, the particle compositions determined by SP-ICP-TOF-MS closely mirror the nominal compositions.

CONCLUSION

SP-ICP-TOF-MS is able to characterize particulates generated from steels down to the femtogram scale and is sensitive to the metallic matrix and to oxide-derived particulates liberated during sample preparation. The elements preferentially colocated with Y differ systematically between PM2000 and 14YWT in a manner that aligns with the known microstructural characteristics of each alloy, supporting a physical origin for the observed trends. In addition, particle generation method affects the resultant particulates. Grinding operations yielded a larger relative detection frequency of Al- and Ti- particulates than cutting operations and also promoted the separation of Y-bearing nanoclusters from the underlying matrix compared to cutting operations. Together, these results demonstrate that SP-ICP-TOF-MS is a robust, particle-resolved tool for disentangling multiple particulate populations in complex steel systems and for linking detected particle chemistry to alloy microstructure and processing history.

CONFLICTS OF INTEREST

There are no conflicts to declare.

ACKNOWLEDGMENTS

This research was funded by the US Department of Energy.

View Article Online
DOI: 10.1039/D6JA00117C

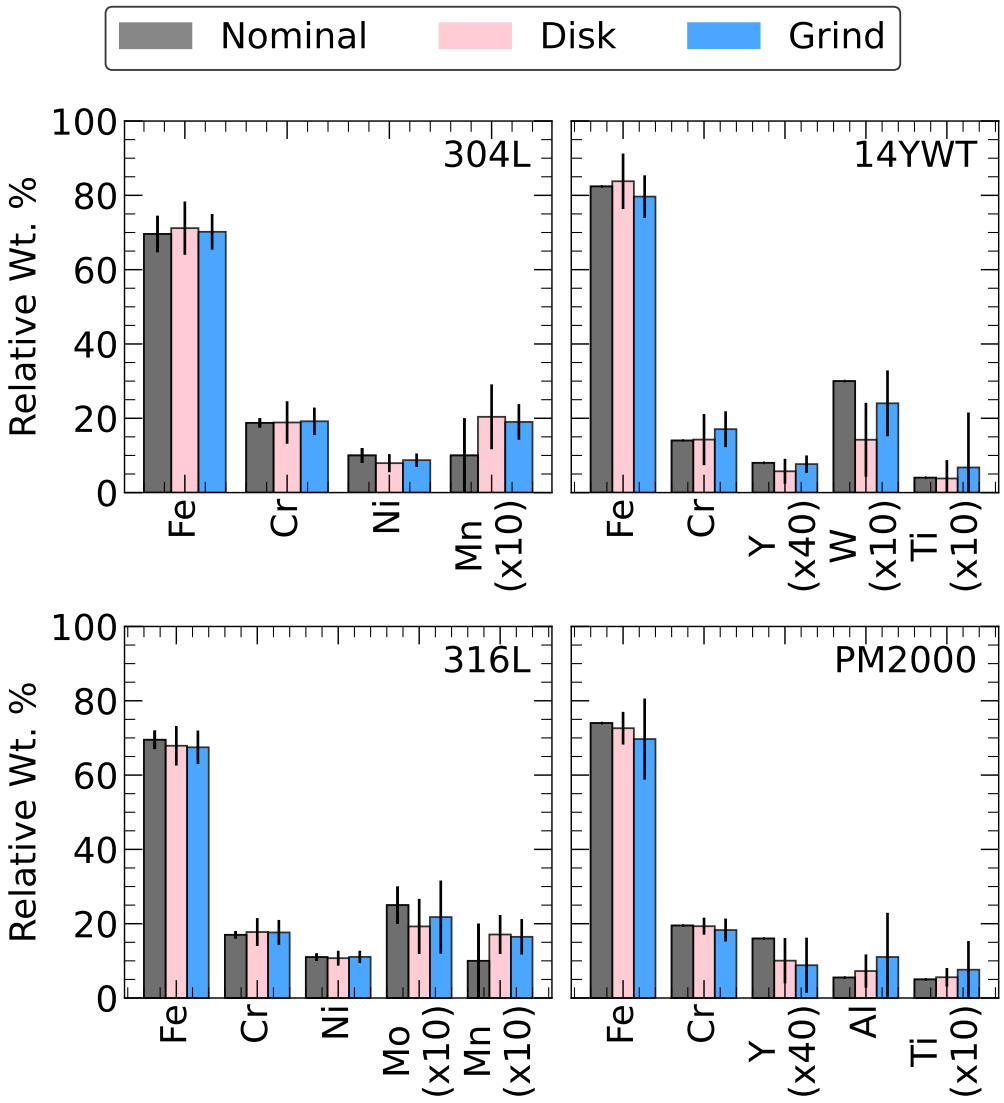

FIG. 4. Nominal compositions compared to compositions extracted by SP-ICP-TOF-MS. For the nominal compositions, the error bars represent the range of expected values. For the values extracted by SP-ICP-TOF-MS the error bars represent the standard deviation of the extracted values. Compositions from SP-ICP-TOF-MS were extracted for Fe content above $L_{D,sp,Fe,Fe-M}$. Overall, the SP-ICP-TOF-MS extracted values agree well with the nominal values, although significant scatter is evident in the PM2000 Al content, most likely because of the high preparation-induced background of Al.

DECLARATION OF GENERATIVE AI AND AI-ASSISTED TECHNOLOGIES IN THE MANUSCRIPT PREPARATION PROCESS

During the preparation of this work, the authors used ChatGPT to assist with text refinement and language streamlining after completing an initial draft. After using these tools, the authors reviewed and edited the content as needed. The authors take full responsibility for the content of the published article.

DATA AVAILABILITY STATEMENT

The data that support the findings of this study will be made openly available in a public repository upon acceptance of the manuscript.

AUTHOR CONTRIBUTIONS

Z. E. Brubaker: formal analysis, visualization, project administration, validation, writing – original draft. S. E. Szakas: investigation, formal analysis, validation, methodology, data curation. D. H. Moseley: resources. J. Hewitt: conceptualiza-

View Article Online
DOI: 10.1039/D6JA00117C

tion, supervision, funding acquisition, project administration. D. T. Hoelzer: resources. B. T. Manard: methodology, supervision, project administration. All authors contributed to writing – review & editing.

* brubakerze@ornl.gov

[1] O. Borovinskaya, S. Gschwind, B. Hattendorf, M. Tanner, and D. Günther, Analytical Chemistry **86**, 8142 (2014).
[2] A. Gundlach-Graham, in *Analysis and Characterisation of Metal-Based Nanomaterials*, Comprehensive Analytical Chemistry, Vol. 93, edited by R. Milačič, J. Ščančar, H. Goenaga-Infante, and J. Vidmar (Elsevier, 2021) pp. 69–101.
[3] F. Gregar, D. Baron, and T. Pluháček, Journal of Separation Science **48**, e70259 (2025).
[4] F. Loosli, J. Wang, S. Rothenberg, M. Bizimis, C. Winkler, O. Borovinskaya, L. Flamigni, and M. Baalousha, Environ. Sci.: Nano **6**, 763 (2019).
[5] K. Mehrabi, R. Kaegi, D. Günther, and A. Gundlach-Graham, Environ. Sci.: Nano **8**, 1211 (2021).
[6] G. D. Bland, M. Battifarano, Q. Liu, X. Yang, D. Lu, G. Jiang, and G. V. Lowry, Environmental Science & Technology Letters **10**, 1023 (2023).
[7] J. S. Stanberry, S. E. Szakas, H. B. Andrews, L. Hendriks, B. W. Ticknor, R. A. Bergin, S. K. Tazik, P. Kegler, S. Neumeier, N. A. Zirakparvar, D. R. Dunlap, and B. T. Manard, Talanta **297**, 128578 (2026).
[8] S. E. Szakas and A. Gundlach-Graham, J. Anal. At. Spectrom. **39**, 1874 (2024).
[9] F. Tou, M. M. Nabi, J. Wang, M. Erfani, E. Goharian, J. Chen, Y. Yang, and M. Baalousha, Environ. Sci.: Nano **9**, 3859 (2022).
[10] A. Azimzada, J. M. Farner, I. Jreije, M. Hadioui, C. Liu-Kang, N. Tufenkji, P. Shaw, and K. J. Wilkinson, Frontiers in Environmental Science **8** (2020), 10.3389/fenvs.2020.00091, cited by: 42; All Open Access, Gold Open Access, Green Open Access.
[11] S. Bevers, M. D. Montaño, L. Rybicki, T. Hofmann, F. von der Kammer, and J. F. Ranville, Frontiers in Environmental Science **8** (2020), 10.3389/fenvs.2020.00084, cited by: 28; All Open Access, Gold Open Access, Green Open Access.
[12] T. Erhardt, C. M. Jensen, O. Borovinskaya, and H. Fischer, Environmental Science & Technology **53**, 13275 (2019).
[13] L. Hendriks, A. Gundlach-Graham, and D. Günther, CHIMIA **72**, 221 (2018).
[14] L. Hendriks, A. Gundlach-Graham, and D. Günther, J. Anal. At. Spectrom. **34**, 1900 (2019).
[15] A. Praetorius, A. Gundlach-Graham, E. Goldberg, W. Fabienke, J. Navratilova, A. Gondikas, R. Kaegi, D. Günther, T. Hofmann, and F. von der Kammer, Environ. Sci.: Nano **4**, 307 (2017).
[16] M. M. Nabi, J. Wang, and M. Baalousha, Chemosphere **263**, 128261 (2021).
[17] A. Gondikas, F. von der Kammer, R. Kaegi, O. Borovinskaya, E. Neubauer, J. Navratilova, A. Praetorius, G. Cornelis, and T. Hofmann, Environ. Sci.: Nano **5**, 313 (2018).
[18] D. Mozhayeva and C. Engelhard, J. Anal. At. Spectrom. **35**, 1740 (2020).
[19] A. J. Goodman, H. Karkee, S. Huang, K. Pfaff, Y. D. Kuiper, Z. Chang, A. Gundlach-Graham, and J. F. Ranville, Chemical Geology **671**, 122498 (2025).
[20] L. G. Jahn, G. D. Bland, L. W. Monroe, R. C. Sullivan, and M. E. Meyer, Aerosol Science and Technology **55**, 571 (2021), https://doi.org/10.1080/02786826.2021.1874610.
[21] T. L. Taylor, M. Strait, and A. Gundlach-Graham, Analytical Chemistry **96**, 20535 (2024).
[22] M. Tharaud, L. Schlatt, P. Shaw, and M. F. Benedetti, J. Anal. At. Spectrom. **37**, 2042 (2022).
[23] A. Hegetschweiler, O. Borovinskaya, T. Staudt, and T. Kraus, Analytical Chemistry **91**, 943 (2019).
[24] S. Naasz, S. Weigel, O. Borovinskaya, A. Serva, C. Cascio, A. K. Undas, F. C. Simeone, H. J. P. Marvin, and R. J. B. Peters, J. Anal. At. Spectrom. **33**, 835 (2018).
[25] R. L. Buckman Johnson, H. Karkee, and A. Gundlach-Graham, J. Anal. At. Spectrom. **40**, 1658 (2025).
[26] H. Karkee, C. Kyte, and A. Gundlach-Graham, J. Anal. At. Spectrom. **39**, 1551 (2024).
[27] J. Zhao, Z. Liu, B. Wang, Q. Song, Y. Cai, A. M. Khan, Y. Wan, and X. Ren, Journal of Manufacturing Systems **70**, 395 (2023).
[28] H. Dawson, J. Hughes, and E. Jimenez-Melero, Fusion Engineering and Design **204**, 114528 (2024).
[29] J. Schneibel, M. Heilmaier, W. Blum, G. Hasemann, and T. Shanmugasundaram, Acta Materialia **59**, 1300 (2011).
[30] H. J. Jung, D. J. Edwards, R. J. Kurtz, T. Yamamoto, Y. Wu, and G. R. Odette, Journal of Nuclear Materials **484**, 68 (2017).
[31] J. Schneibel, C. Liu, M. Miller, M. Mills, P. Sarosi, M. Heilmaier, and D. Sturm, Scripta Materialia **61**, 793 (2009).
[32] G. Odette, M. Alinger, and B. Wirth, Annual Review of Materials Research **38**, 471 (2008).
[33] D. Hoelzer, J. Bentley, M. Sokolov, M. Miller, G. Odette, and M. Alinger, Journal of Nuclear Materials **367-370**, 166 (2007), proceedings of the Twelfth International Conference on Fusion Reactor Materials (ICFRM-12).
[34] D. Hoelzer, K. Unocic, M. Sokolov, and T. Byun, Journal of Nuclear Materials **471**, 251 (2016).
[35] N. Hansen, X. Huang, D. {Juul Jensen}, E. Lauridsen, T. Leffers, W. Pantleon, T. Sabin, and J. Wert, English*Recrystallization - Fundamental aspects and relations to deformation microstructure. Proceedings* (Risø National Laboratory, 2000).
[36] Y. Wang, J. Lin, B. Liu, Y. Chen, D. Li, H. Wang, and Y. Shen, Philosophical Magazine **101**, 2514 (2021).
[37] M. K. Miller, C. M. Parish, and Q. Li, Materials Science and Technology **29**, 1174 (2013), https://doi.org/10.1179/1743284713Y.0000000207.
[38] B. T. Manard, V. C. Bradley, C. D. Quarles, L. Hendriks, D. R. Dunlap, C. R. Hexel, P. Sullivan, and H. B. Andrews, Nanomaterials **13** (2023), 10.3390/nano13081322.
[39] A. Gundlach-Graham, S. Harycki, S. E. Szakas, T. L. Taylor, H. Karkee, R. L. Buckman, S. Mukta, R. Hu, and W. Lee, J. Anal. At. Spectrom. **39**, 704 (2024).
[40] H. E. Pace, N. J. Rogers, C. Jarolimek, V. A. Coleman, C. P. Higgins, and J. F. Ranville, Analytical Chemistry **83**, 9361 (2011).
[41] H. E. Pace, N. J. Rogers, C. Jarolimek, V. A. Coleman, E. P. Gray, C. P. Higgins, and J. F. Ranville, Environmental Science & Technology **46**, 12272 (2012).
[42] A. Gundlach-Graham, L. Hendriks, K. Mehrabi, and D. Günther, Analytical Chemistry **90**, 11847 (2018).
[43] S. E. Szakas, R. Lancaster, R. Kaegi, and A. Gundlach-Graham, Environ. Sci.: Nano **9**, 1627 (2022).

View Article Online
DOI: 10.1039/D6JA00117C

Data Availability Statement

The data that support the findings of this study will be made openly available in a public repository upon acceptance of the manuscript.